Analysis of the F-1 Acoustic Liner

C. L. Oberg* and N. M. Kuluva†
Rocketdyne/North American Rockwell Corporation, Canoga Park, Calif.

An analytical study was performed to re-evaluate data obtained during the F-1 Acoustic Absorber program. The acoustic liner had failed to produce substantial improvements in stability. Oscillatory pressure, temperature, and gas sampling data obtained from liner firings were employed to calculate the damping produced by the liner and the potential for increasing the damping by varying the liner dimensions. The results indicate the damping can be substantially increased. The liner damping was predicted by calculating temporal damping-coefficient contributions due to the liner.

Nomenclature

B = defined by Eq. (8)
c = isentropic sound velocity
$G(\mathbf{r}|\mathbf{r}_0)$ = Green's function
j = $(-1)^{1/2}$
$J_m(\ )$ = Bessel function of first kind and order m; $J_m'(\ ) = dJ_m/d(\ )$
k = β/c
L,l = chamber and aperture lengths, respectively
l_e = equivalent aperture length
$\hat{M}_a$ = peak aperture Mach number
m = angular index of instability modes
$\mathbf{N}$ = unit normal vector pointed outward
n = radial index of instability mode
P = time averaged pressure
$\tilde{p}$ = oscillatory pressure (complex)
$\tilde{p}_0$ = $\tilde{p}$ at linear surface
R = $r_w c_a/r_0 c$, also resistance
r = radial coordinate
r_i,r_0 = inner and outer radii of resonator cavity
r_w = radius of chamber wall
Δr = backing distance, $r_0 - r_i$
S = surface area
t = time
$\tilde{\mathbf{u}}$ = oscillatory velocity vector
V = volume of chamber, or resonator cavity
$Y_m(\ )$ = Bessel function of second kind and order m; $Y_m'(\ ) = dY_m/d(\ )$
z,z_w = impedance and liner impedance, respectively
α = damping coefficient, imaginary part of β
α_{mn} = root of $dJ_m(\alpha_{mn})/d\alpha_{mn} = 0$
α_N = α of Nth mode
β = complex angular frequency, $\beta = \omega + j\alpha$
γ = heat capacity ratio
Γ = empirical resistance coefficient, $d\theta_a/d\hat{M}_a$
ζ = specific impedance, $z_a/\sigma\rho c$
η_0 = $\omega_0 r_w/c$
$\eta_{\nu mn}$ = $\{\alpha_{mn}^2 + \nu^2\pi^2 r_w/L^2\}^{1/2}$
θ = specific resistance; also, angular coordinate
θ_a = specific aperture resistance, $R/(\rho c)_a$
θ_1 = specific liner resistance $(\rho_a c_a/\rho c)\theta_a$
ρ = time-averaged density in combustion chamber
ρ_a = time-averaged density in aperture
σ = open-area fraction based on liner surface
σ_1 = open-area fraction based on liner surface from cavity side
ϕ = $\beta r_w/c$
ω = angular frequency, real part of β

Subscripts

a,c = aperture and cavity conditions, respectively

Presented as Paper 70-619 at the AIAA 6th Propulsion Joint Specialist Conference, San Diego, Calif., June 15–19, 1970; received July 13, 1970; revision received July 1, 1970. Information contained herein was developed under NASA-MSFC Contract NAS8-21354; R. J. Richmond, Technical Monitor.

* Manager, Combustion, Advanced Programs., Member AIAA.
† Member of Technical Staff.

Introduction

THE effectiveness of acoustic liners in preventing acoustic modes of combustion instability in rocket engines has been demonstrated repeatedly. Nevertheless, it is still difficult to accurately calculate the stabilizing influence of a liner. This paper describes methods that have been developed to evaluate the damping produced by an acoustic liner which are believed to be more effective than previously used methods. The paper is based on an analytical program[1] directed toward re-evaluation of data obtained previously during a test firing program[2] in which an acoustic liner was designed and tested in the F-1 rocket engine. The liner (Fig. 1) proved to be largely ineffectual; no substantial improvements in stability were observed. It was tested with four injector types, each of which had well-established stability characteristics. The 2600 apertures in the liner were formed by drilling $\frac{3}{16}$ in-diam holes through the wall of an uncooled, solid wall thrust chamber. Toroidal resonator cavities were formed by welding 10 shells around the thrust chamber with 3 rows of apertures leading into each. None of these cavities was partitioned to prevent flow in the circumferential direction. The resonator "backing distance," $\Delta r = \sigma V/S$, was 1.065 in. in the torus adjacent to the injector, while the backing distance for the remaining cavities was 1.64 in.

Liner Impedance Calculations

Calculation of the acoustic impedance of the liner was possible because simultaneous measurements of oscillatory pressure were made at the liner surface and within the resonator cavities of the liner at several locations. In addition, probes were used to measure the transverse gas velocity and withdraw gas samples for subsequent compositional analyses. Thermocouples were used to measure gas temperatures in the apertures and resonator cavities of the liner.

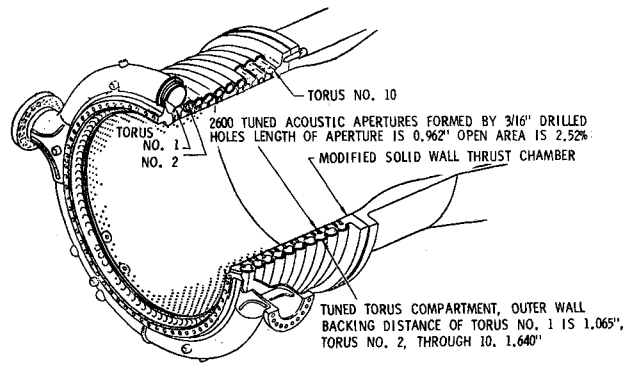

Fig. 1 F-1 acoustic liner design.

The acoustic impedance of the apertures in a liner can be determined from these oscillatory pressure measurements by employing a technique used by Sivian in 1935 when he discovered the nonlinearities in the acoustic resistance of an orifice.[3]

The amplitude ratio and phase angle between the oscillatory pressures at the liner surface and in the resonator cavity specify the ratio between the impedance of the liner and the impedance of the resonator cavity alone. Because the impedance of the resonator cavity is known with reasonable confidence, the liner impedance may be determined.

The impedance of a Helmholtz resonator is

$$\tilde{p}_0/\tilde{u}_a = z_a + z_c \tag{1}$$

whereas, the impedance of the resonator cavity is

$$\tilde{p}_c/\tilde{u}_a = z_c \tag{2}$$

These equations may be combined to eliminate $\tilde{u}_a$,

$$\tilde{p}_0/\tilde{p}_c = 1 + (z_a/z_c) \tag{3}$$

where $\tilde{p}_0$ and $\tilde{p}_c$ are the oscillatory pressures at the liner surface and within the resonator cavity, respectively.

The impedance of an annular resonator cavity of the kind used on the F-1 engine is given by

$$z_c = -j\rho c\sigma_1 \frac{J_m\left(\frac{\omega r_i}{c}\right) Y_m'\left(\frac{\omega r_0}{c}\right) - Y_m\left(\frac{\omega r_i}{c}\right) J_m'\left(\frac{\omega r_0}{c}\right)}{J_m'\left(\frac{\omega r_i}{c}\right) Y_m'\left(\frac{\omega r_0}{c}\right) - Y_m'\left(\frac{\omega r_i}{c}\right) J_m'\left(\frac{\omega r_0}{c}\right)} \tag{4}$$

This expression was obtained by solving the wave equation for an annular cavity with the outer boundary being assumed rigid. Equation (4) may be simplified if the radial thickness of the annulus is small compared to a wavelength. In that event, the Bessel functions corresponding to the inner radius may be approximated by the initial terms in a Taylor series expansion about the outer radius. Thereby, Eq. (4) may be reduced to

$$z_c = -j\frac{\gamma P_0\sigma_1}{\omega\Delta r}\frac{(\omega r_0/c_c)^2}{(\omega r_0/c_c)^2 - m^2} \tag{5}$$

Equations (3) and (5) can be used directly to calculate the aperture impedance, z_a, from the amplitude and phase angle data. However, these expressions can be written in a more clearly familiar form by introducing expressions for the resonant frequency and aperture reactance.

The aperture impedance is usually written in the form

$$z_a = R + j\rho_a\omega l_e \tag{6}$$

The undamped resonant frequency is defined as the frequency at which the reactance of the liner is zero; thereby, the following expression is readily obtained:

$$(\omega_0 r_0/c_c)^2 = m^2 + c_a^2\sigma_1 r_0^2/c_c^2 l_e\Delta r \tag{7}$$

The liner impedance may then be written as

$$z = R + j\rho_a l_e\omega B(B^{-1} - B) \tag{8}$$

where

$$B = \left[\frac{(\omega_0 r_0/c_c)^2 - m^2}{(\omega r_0/c_c)^2 - m^2}\right]^{1/2}$$

With $B = \omega_0/\omega$, Eq. (8) is the usual impedance expression for Helmholtz resonators. The factor B arises, of course, because of the lack of partitions in the resonator cavities. Further, with the definition

$$\tilde{p}_0/\tilde{p}_c = r_p e^{i\psi} \tag{9}$$

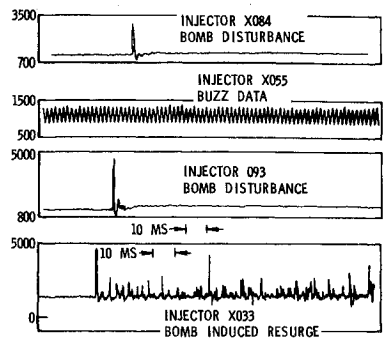

Fig. 2 Typical oscillatory pressure data.

Equation (3) becomes

$$r_p\cos\psi = (B - B^{-1})/B \tag{10}$$

$$r_p\sin\psi = R/\rho_a\omega B^2 l_e \tag{11}$$

These equations can be used to calculate the quantities B and then $R/\rho_a\omega l_e$ directly from the oscillatory pressure data.

If $c_a = c_c$, or c_a/c_c is known, and if the effective length of the aperture is estimated independently, c_a and the liner resonant frequency can be calculated from the value of B because the remaining parameters should be known. The specific aperture resistance, $\theta_a = R/\rho_a c_a$, may be subsequently calculated directly. The approach is simpler for a partitioned resonator cavity because $m = 0$ and, therefore, $B = \omega_0/\omega$.

After examining the data from the F-1 liner, it became evident that most of the phase angle data were of insufficient accuracy to use. To circumvent this problem, c_a was estimated from the temperature and gas sampling data, c_a and c_c were assumed equal, and the effective aperture length was estimated by adding a calculated end correction to the physical length. By employing these estimates, the phase angle could be calculated or eliminated from the impedance calculation. As long as θ_a is reasonably high, its calculation is not overly sensitive to the estimated c_a. Therefore, the inability to employ the phase-angle data was not a serious handicap.

Typical oscillatory chamber pressure records obtained from tests using the four different injectors are shown in Fig. 2. These data were processed for the impedance calculation with a spectral analysis technique; typical results are shown in Fig. 3.

The amplitude, temperature, and gas sampling data were used to calculate the liner impedance. The specific resistance results were expected to be described by a relationship of the form: $\theta_a = \Gamma\hat{M}_a$, where $\hat{M}_a = |\tilde{p}_c|/c_a|z_c|$. The empirical coefficient Γ is assumed to include the steady cross flow effect.[4] The results correlated on this basis are shown in Fig. 4. The results are scattered but are believed to be sufficient to define a mean Γ, i.e., the slope of a straight line passing through the origin. This correlation ($\Gamma = 3.5$) was used to specify θ_a for the damping calculations.

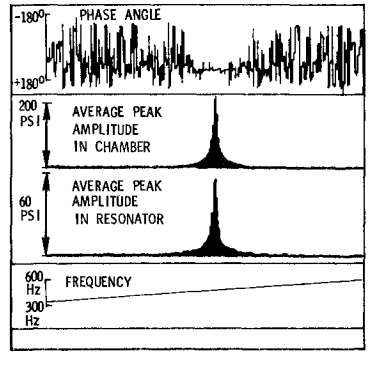

Fig. 3 Typical amplitude and phase results.

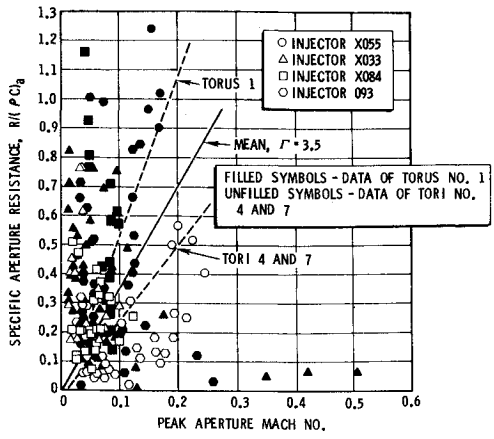

Fig. 4 Variation of specific aperture resistance with the amplitude of the oscillatory Mach number in the aperture.

Damping Calculations

The damping contributed by the liner was estimated by calculating a damping coefficient for the liner. The relevance of the damping coefficient has been demonstrated in studies of solid propellant instability[5,6] and also in Refs. 1 and 7. In addition, it is shown therein that the over all temporal damping coefficient, α_N, is given by $\alpha_N \simeq \Sigma_i \alpha_{Ni}$, where the index i refers to the various contributory processes, and the time dependence of the oscillatory motion has been assumed to be $e^{j\beta_N t}$, where $\beta_N = \omega_N + j\alpha_N$. Further, each α_{Ni} can be adequately estimated by a calculation which ignores the remaining contributions. Consequently, the damping coefficient α was calculated by solving the wave equation for the chamber. Because only the damping contributed by the liner was desired, the effects of chamber through-flow, combustion, and losses other than the liner were ignored.

If the acoustic impedance of the liner is assumed to be uniform, the wave equation can be solved in a straightforward fashion. For a full-length liner, by the method of separation of variables to give, for standing waves

$$\tilde{p} = \hat{p} e^{j\beta t} \cos m\theta J_m(\phi r/r_w) \tag{12}$$

where ϕ is a root of the characteristic equation

$$[J_m(\phi)]/J_m'(\phi) = j\zeta \tag{13}$$

and ζ is the specific impedance of the liner ($\zeta = z/\sigma\rho c$). The various temporal damping coefficients are determined by solving the characteristic equation for the complex eigenvalues; the real part of each eigenvalue specifies the resonant frequency, and the imaginary part specifies the damping coefficient corresponding to that mode.

Equation (13) has been solved for several cases by employing Newton's method as a numerical root-finding technique. However, some difficulty was encountered because the Bessel functions are rather strongly dependent on their argument. Consequently, convergence to any root was not very satisfactory and, a more well-behaved representation was sought.

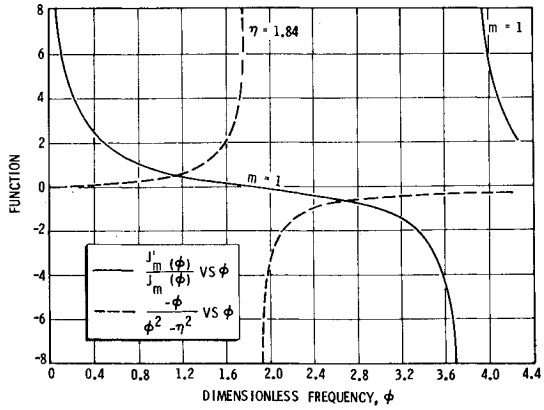

Fig. 5 Frequencies for undamped liner.

Such a representation was obtained with the aid of Green's functions. The wave equation and boundary conditions for a cylindrical chamber with a full-length liner may be rewritten as an integral equation,[8]

$$\tilde{p}(\mathbf{r}) = \int_S G(\mathbf{r}|\mathbf{r}_0)\mathbf{N}\cdot\nabla p(\mathbf{r}_0)dS_0 \tag{14}$$

where the Green's function may be written as

$$G(\mathbf{r}|\mathbf{r}_0) = \sum_{m,n,\nu} \frac{J_m\left(\frac{\alpha_{mn}r}{r_w}\right) J_m\left(\frac{\alpha_{mn}r_0}{r_w}\right) \cos m\theta \cos m\theta_0 \cos\frac{\nu\pi z}{L} \cos\frac{\nu\pi z_0}{L}}{\frac{\pi r_w^2 L}{\epsilon_m \epsilon_\nu} J_m^2(\alpha_{mn}) \left(\frac{\alpha_{mn}^2 - m^2}{\alpha_{mn}^2}\right)(\eta_{mn\nu}^2 - k^2)} \tag{15}$$

where the subscript 0 refers to source coordinates. However,

$$\mathbf{N}\cdot\nabla\tilde{p}(r_0) = -jk\tilde{p}(r_0)/\zeta \tag{16}$$

and, further, because the boundary conditions are uniform, $\tilde{p}(r)$ is given by Eq. (12).

By inserting Eq. (12) and Eq. (15) into Eq. (14) and integrating over the liner surface, the following characteristic equation was obtained

$$\phi \sum 2\alpha_{\bar{m}n}^2/[(\alpha_{\bar{m}n}^2 - \bar{m}^2)(\eta_{\bar{m}\bar{\nu}n}^2 - \phi^2)] = j\zeta \tag{17}$$

For tangential and radial modes, $\eta_{\bar{m}\bar{\nu}n}^2 = \alpha_{\bar{m}n}^2$ (because $\nu = 0$). Equation (17) with $\nu = 0$ must necessarily be equal to Eq. (13). Further, Eq. (17) is an exact equation insofar as the uniform impedance approximation is valid.

The series in Eq. (17) converges rapidly and can be adequately approximated in truncated form after removal of the specific mode of interest from the series, i.e., $n = \bar{n}$. This equation was readily solved by application of Newton's method and with the aid of a time sharing computer. The equation is well behaved and little difficulty has been encountered in obtaining results. Employing the impedance results given previously, the liner damping coefficient was calculated from Eq. (17).

One feature of the damping coefficient calculations was the prediction of mode splitting; the normal modes of the chamber are split into two modes by the influence of the liner. This effect is most easily seen for an undamped liner, $\theta_1 = 0$. For this case, the eigenvalues or resonant frequencies can be determined by simply plotting each side of the characteristic equation, Eq. (13), as a function of ϕ. Such a plot is shown in Fig. 5. The dashed curves represent the indicated impedance expression; this expression does not correspond to the F-1 liner, however, similar results were obtained for that liner. The solid curves represent the Bessel function ratio. Intersections of the solid and dashed curves for common values of m correspond to solutions to the characteristic equation.

Initially, a set of exploratory calculations was made, the liner being assumed to operate at nominal conditions and the specific surface resistance, θ_1, was treated as a parameter. The calculated damping coefficients for the lowest, several modes are shown in Fig. 6 for the F-1 liner. As indicated, the normal modes of oscillation were found to split into two modes, one with a frequency near the resonant frequency of the liner and the other near the normal frequency. To retain the usual notation for these modes, the two branches from each normal mode are denoted "lower" and "upper" corresponding to the low- and high-frequency branches from that mode.

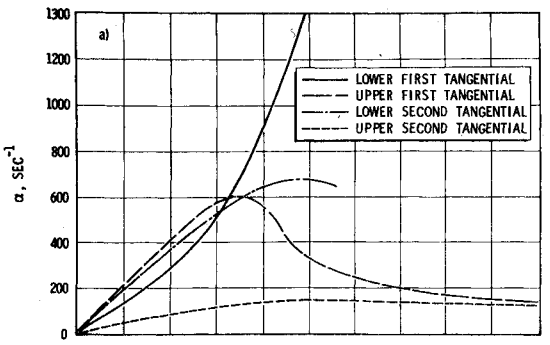

Fig. 6a Predicted damping for existing liner.

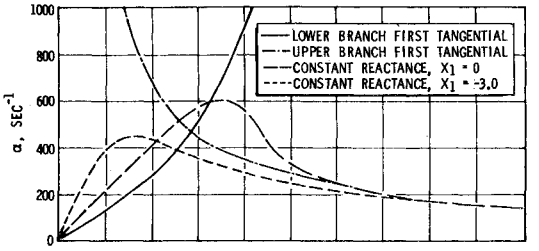

Fig. 6b Comparison of damping predictions with frequency dependent and independent liner reactances.

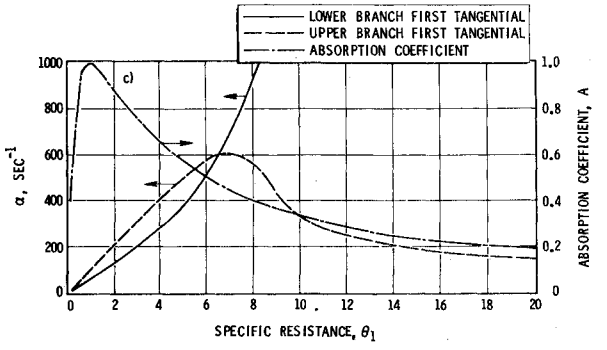

Fig. 6c Comparison of damping predictions from the absorption coefficient and the damping coefficient.

Stability considerations are complicated somewhat by the mode splitting that occurs, because the stabilizing influence of the liner on all modes in the frequency range of interest must be considered. The mode splitting increases the number of modes that must be considered.

The results shown in Fig. 6a suggest that the optimum specific resistance is ~7 for modes with frequencies near the normal first tangential mode. The damping is low for the upper branch of the second tangential mode, but that mode is presumed to be less strongly driven because of its higher frequency.

Predicted damping coefficients for the first tangential modes and for liners with axially directed partitions were 5 to 20% higher than the same damping coefficients for liners without partitions.

Similar calculations were made to compare damping- and absorption-coefficient predictions of damping. The results, shown in Figs. 6b and 6c, indicate that the absorption and damping coefficients exhibit the same trends only if the liner reactance is treated as independent of frequency. However, this reactance is known to depend strongly on frequency near resonance.

Subsequently, the impedance results from the engine were used to calculate the damping coefficients to be expected from the current liner design. The characteristic equation was solved with an impedance expression of the form

$$\zeta = \theta_1 + jK_1\{\phi(\phi^2 - \eta_0^2)/[\phi^2 - m^2R^2]\} \qquad (18)$$

where

$$\eta_0 = \frac{\omega_0 r_w}{c} = \frac{c_a}{c}\frac{r_w}{r_0}\left[\frac{\sigma_1 r_0^2}{\Delta r l_e} + m^2\right]^{1/2}$$

$$\theta_1 = \frac{(\rho c)_a}{\rho c}\frac{\Gamma \hat{M}_a}{\sigma} \qquad K_1 = \frac{(\rho c)_a}{\rho c}\frac{c}{c_a}\frac{l_e}{\sigma r_w}$$

The peak aperture Mach number, $\hat{M}_a$, was calculated from the expression

$$\hat{M}_a = \frac{\hat{p}\sigma}{\rho|\zeta|} = \frac{c}{c_a}\left(\frac{\hat{p}}{\gamma P}\right)\frac{\sigma}{|\zeta|} \qquad (19)$$

Equations (19) and (20) can be combined to give a fourth-order equation in $\hat{M}_a$. This fourth-order equation and the characteristic equation were solved simultaneously by means of Newton's method to obtain the eigenvalues. The damping coefficients were calculated directly from the imaginary part of the eigenvalues. Because the liner impedance was assumed to be independent of position, an average pressure amplitude must be used to calculate the peak aperture Mach number. The root-mean-square average amplitude appears appropriate.

The magnitude of the pressure amplitude most appropriate for liner calculations is not well-defined. Most of the calculations shown herein were made for rms amplitudes of 4.8 and 12% of chamber pressure which correspond to peak-to-peak amplitudes of 14 and 34%, respectively. These levels were chosen rather arbitrarily to indicate the amplitude effect; however, these are believed to be in the most appropriate range. Acoustic equations (including the absorption coefficient) should not be used above peak-to-peak levels of 20 or 30%[5]; conversely, amplitudes less than 5% are within the combustion noise. These levels were used as guidelines for selecting design amplitudes.

Calculated damping coefficients for the existing liner and over a range of mean aperture temperatures are shown in Fig. 7a for two pressure amplitudes. The mean aperture temperatures measured with each of the four injectors are indicated as well. These curves provided a baseline with which to compare subsequent calculations, in which the potential for in-

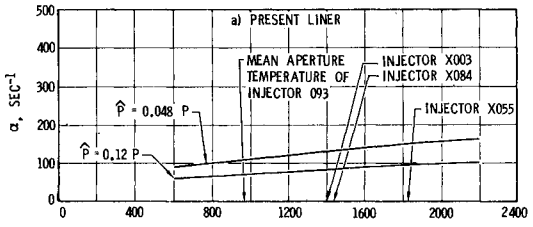

Fig. 7a Predicted damping coefficients for the first tangential mode with present F-1 liner configurations (Γ = 3.5).

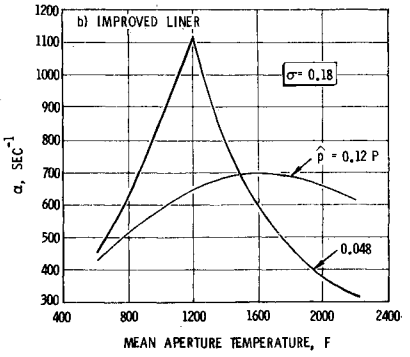

Fig. 7b Predicted damping coefficients for the first tangential mode with improved F-1 liner configurations (Γ = 3.5).

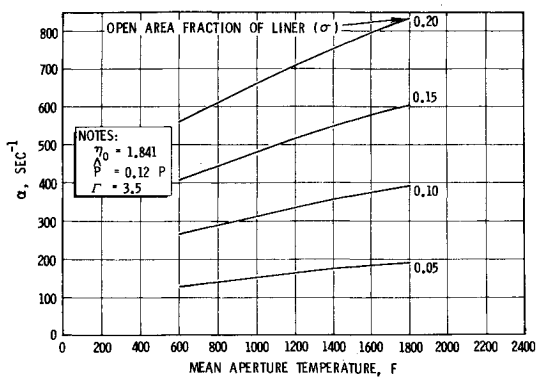

Fig. 8 Variation of predicted damping coefficients with aperture temperature and open area (upper-branch first-tangential mode).

creasing the liner damping by varying the liner configuration was investigated. The empirically determined aperture resistance expression ($\Gamma = 3.5$) was assumed to remain valid with the new liner dimensions.

The effect of increased open area is shown in Fig. 8. The dimensionless resonant frequency, η_0, was assumed fixed for these calculations rather than fixed cavity dimensions. Thus, the cavity volume was varied to compensate for aperture temperature changes so that the resonant frequency was fixed. An aperture diameter of 0.5 in was selected for additional calculations, the corresponding open area being 18%.

For an 18% open area and increased cavity volume, a liner configuration was selected which would give near-maximum damping. Predicted damping coefficient curves for this configuration are shown in Fig. 7b. The predicted α for this configuration was 680 sec^{-1} at $T_a = 1400°F$ and $\hat{p} = 0.12P$ (rms). This represents a seven-fold increase in α over the existing liner design. In addition, α remains reasonably large if $\hat{p}$ is reduced to 0.048P (rms). However, the sensitivity to temperature variations is much larger. Note that these curves are for fixed liner dimensions, whereas, Fig. 8 was developed for fixed resonant frequency so that the curves (Fig. 8) are less sensitive to temperature variations.

Further calculations were based on an aperture temperature of 1400°F, which is near the average of the previously measured liner temperatures. An important alternative, from the standpoint of modifications to the existing liner, is the potential for increased damping from enlarging only the aperture diameter. A set of calculations was made for this case; the results are shown in Fig. 9. These curves show that a substantial increase in damping can be obtained simply by increasing the aperture diameter. Note that these results imply that maximum damping would be obtained with a liner resonant frequency approximately twice the instability frequency, because the resonant frequency is nearly proportional to $\sigma^{1/2}$. This effect occurs with volume-limited con-

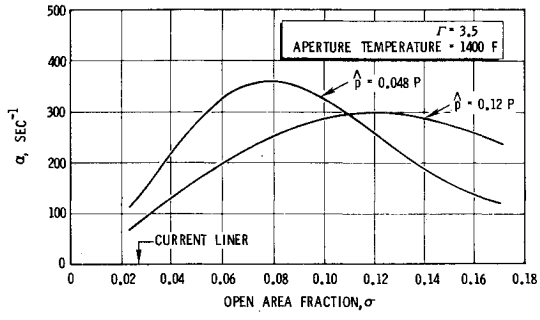

Fig. 9 Variation of first-tangential mode damping (upper branch) with open area when only the aperture diameter is changed from current configuration.

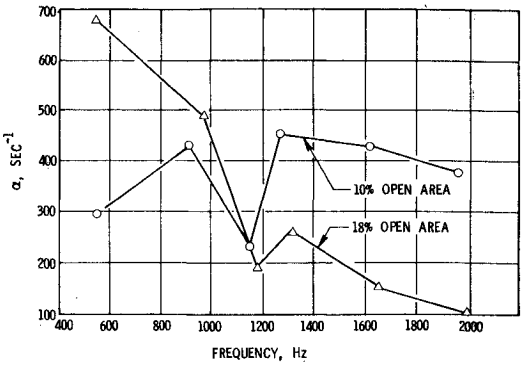

Fig. 10 Predicted damping coefficients for various modes ($\hat{p} = 0.12P$).

figurations because the damping is related to both the tuning and the open area available for removing energy.

These results show that an α of 300 sec^{-1} (for 12% rms amplitude) can be obtained with larger apertures. Additional results, which are not shown, indicate a further increase to 370 sec^{-1} is possible by increasing the aperture length as well as the diameter but with fixed cavity volume.

Even though the F-1 liner was principally intended to damp modes with frequencies near the first-tangential frequency, the effectiveness against other modes is also of interest. Therefore, calculations were made to determine α's for modes in the 0- to 2000-Hz frequency range (Fig. 10). The two sets of points have been connected by lines for convenience of the reader; these lines have no meaning in terms of damping because only discrete frequencies are obtained from the calculation. The frequencies are determined by the acoustics of the lined chamber and cannot be varied arbitrarily. The frequencies shown are based on an unlined first-tangential frequency of 550 Hz.

Conclusions

The experimental and analytical techniques applied and developed during this study to determine liner impedance and damping are believed valuable for liner design and for developing a better understanding of liner behavior. Results from the impedance determination, employing the oscillatory pressure data and the temperature and gas sampling data, are believed to be of considerable significance, even though the resistance results are widely scattered. The resistance data are sufficient to define the over-all magnitude of the resistance and the general trend of its variation with peak aperture velocity. Although these kinds of measurements are both difficult to make and to interpret, they provide a valuable technique for determining at least approximately, the liner impedance that exists during a hot firing. Therefore, the use of this experimental technique to evaluate and improve new liner designs is recommended.

The temporal damping coefficient is recommended as a criterion for liner design. The analytical techniques described herein can be employed to calculate the damping coefficient with relative ease. Further, it is believed to be a much better measure of the damping capability of a liner than the absorption coefficient. While a number of simplifications have been introduced, these can be systematically removed with further development. For example, the effects of impedance nonuniformity and steady chamber flow can be included by a modified integral formulation, similar to Eq. (14).

Further, results from the damping calculations clearly indicate that a substantial increase in liner damping from the F-1 liner can be obtained by increasing the liner dimensions (cavity volume and aperture length and/or diameter) within moderate bounds.

References

[1] Oberg, C. L. and Kuluva, N. M., "Acoustic Liners for Large Engines," R-7792, March 1969, Rocketdyne/North American Rockwell Corp., Canoga Park, Calif.

[2] "F-1 Engine Acoustic Absorber Task, Final Report," R-7911, July 1967, Rocketdyne/North American Rockwell Corp., Canoga Park, Calif.

[3] Sivian, L. J., "Acoustic Impedance of Small Orifices," *The Journal of the Acoustical Society of America*, Vol. 7, Oct. 1935, pp. 94–101.

[4] "A Study of the Suppression of Combustion Oscillations With Mechanical Damping Devices-Final Report," PWA FR-2596, Nov. 1967, Pratt Whitney Aircraft, Florida Research and Development Center, West Palm Beach, Fla.

[5] Hart, R. W. and McClure, F. T., "Theory of Acoustic Instability in Solid Rocket Combustion," *Tenth Symposium (International) on Combustion*, Combustion Inst., Pittsburgh, Pa., 1965, pp. 1047–1065.

[6] Cantrell, R. H. and Hart, R. W., "Interaction Between Sound and Flow in Acoustic Cavities: Mass, Momentum, and Flow Considerations," *The Journal of the Acoustical Society of America*, Vol. 36, No. 4, April 1964, pp. 697–706.

[7] Oberg, C. L., "Combustion Stabilization with Acoustic Cavities," *Journal of Spacecraft and Rockets*, Vol. 8, No. 12, Dec. 1971, to be published.

[8] Morse, P. M. and Ingard, K. U., *Theoretical Acoustics*, McGraw-Hill, New York, 1968, pp. 579–580 and 680.

NOVEMBER 1971 J. SPACECRAFT VOL. 8, NO. 11

Some Three-Body Numerical Solutions for Low-Thrust Orbiter Missions

JOHN S. MACKAY* AND ALFRED C. MASCY*
NASA Advanced Concepts and Missions Division, OART, Moffett Field, Calif.

A "velocity at the sphere of influence" method and an asymptotic matching method of patching together two-body low thrust solutions are compared to a number of three-body numerical results for outer planet orbiter missions. The two patching methods compare well with the numerical three-body results and do not depend on any particular choice for the size of the sphere of influence. The results apply, in a strict sense, only to the operational mode used-high-thrust terminal retro into orbit. Low-thrust spirals are not considered in the three-body analysis. The terminal low-thrust phase of thrusting is almost entirely reverse to the velocity vector during the planet centered phase of the trajectory. This may lead to important simplifications for low-thrust guidance and navigation procedures.

Introduction

STRACK,[1] in a study of three-body effects on optimal low-thrust trajectories, presented a method for patching together two-body low-thrust trajectories which accounted for the actual velocity of the space vehicle as it crosses a planetary sphere-of-influence. This work focused specifically on the Earth departure phase of Earth to Mars trajectories and examined low-thrust, spiral type escape paths as well as high-thrust departure at escape speed followed by low-thrust propulsion on out to Mars. The effect of the gravity of Mars was not considered.

One major result of Strack's work was that accounting for the actual velocity at the sphere-of-influence gave most of the true three-body answer as opposed to using the velocity at an infinite distance (hyperbolic velocity). Further refinements due to the use of a sphere-of-influence for Earth of 300 Earth radii together with propulsion to the sphere were also shown.

One of the purposes of this paper, therefore, is to examine the V_S (velocity-at-the-sphere) method when applied to other low-thrust situations, such as the planetary approach phase for outer planet orbiter missions. Specifically, it will be assumed that a nuclear-electric powered propulsion system is used to help establish large elliptical orbits (eccentricity = 0.95) about the planets Jupiter, Saturn, Uranus and Neptune. Results will then be compared, for a range of transfer times, between some numerical three-body solutions (vehicle, sun and target planet), Strack's V_S method and the asymptotic matching procedure suggested by Breakwell[2] and others.[3,4]

Received Sept. 17, 1970; revision received June 21, 1971.

* Aerospace Engineer, Space Missions and Technology Branch. Member AIAA.

Analysis

The mathematical and numerical techniques used in this paper are essentially identical to those used by Strack.[1] In fact, the same computer program[5] and computer model have been utilized. The main difference is in the method of attack on the problem, which was almost dictated by the problem itself. For example, first two-dimensional, two-body problems were solved and optimized for a given set of propulsion system and launch vehicle parameters. Next, three-dimensional, two-body solutions were found for a convenient set of planetary orbit elements[6] using launch dates in or near the 1980 time period. These results were also optimized with respect to the initial $F/W_o, I_{sp}$, launch vehicle injection speed and planet approach velocity. Finally the target planet gravitational force was introduced and one free initial condition was adjusted until the desired planetary passage distance was achieved. These final computations were not re-optimized.

Planet and Orbit Selection

The planets Jupiter, Saturn, Uranus and Neptune were selected as probable targets for low-thrust missions based on previous mission analyses.[7] Also, orbiter missions were selected because they demand an energy level more appropriate to electric propulsion.

The nominal mission profile selected does not use the electric propulsion system to establish the orbit about the planet.